

Effective learning is accompanied by increasingly efficient dimensionality of whole-brain responses

Evelyn Tang,¹ Marcelo G. Mattar,² Chad Giusti,¹ Sharon L. Thompson-Schill,² and Danielle S. Bassett^{1,3}

¹*Department of Bioengineering, University of Pennsylvania, PA 19104 USA*

²*Department of Psychology, University of Pennsylvania, Philadelphia, PA 19104 USA*

³*Department of Electrical and Systems Engineering, University of Pennsylvania, PA 19104 USA*

(Dated: June, 2017)

Theories and tools to measure the efficiency of neural codes have been important in understanding neural responses to external stimuli. However, similar principles to describe the efficiency of brain responses to tasks demanding higher-order cognitive processes remain underdeveloped. A key domain to study such efficiency is learning, where patterns of activity across the entire brain provide insight into the principles governing the acquisition of knowledge about objects or concepts. We propose a mathematical framework for studying the efficiency of spatially embedded whole-brain states reflected in functional MRI, and demonstrate its utility in describing how human subjects learn the values of novel objects. We find that compared to slow learners, quick learners use a smaller ambient embedding to simultaneously encode higher dimensional patterns of neural responses to stimuli, providing a notion of effective coding most associated with rapid learning. Furthermore, we identify which regions form the strongest neurophysiological drivers of these differences in learning rate, and complement our region-based approach with a voxel-level approach to uncover structure in finer-scale responses. Finally, for a full investigation of complementary geometric approaches, we verify that quick learners develop more assortative responses to stimuli: that is, whole-brain responses that are more easily distinguishable from one another. Our work offers a suite of geometric measures to represent a notion of efficient coding for higher-order cognitive processes, and provide insight into the dimensionality of neural responses characteristic of the successful optimization of reward, that are applicable to the study of cognitive performance more broadly.

INTRODUCTION

The notion of the coding efficiency in sensory systems has been critical to the understanding of neural responses to external stimuli [1, 2]. Such efficiency has often been quantified in relation to the system’s relative optimization of information transfer given biophysical and metabolic constraints. An open question is whether similar principles play a role in higher-level processes such as cognition. What goals and constraints must be balanced to enable cognitive coding efficiency, and how might such efficiency support accurate perceptions and decisions? While efficiency in cognitive coding has been proposed [3, 4], usefully defining this concept remains a challenge [5]; here we provide a mathematical framework to quantify such efficiency in the combined neural responses from distributed brain regions. In learning for instance, information is thought to be integrated across many areas to form representations [6, 7], appreciate abstract value [8], and both prepare and execute appropriate motor responses. Indeed the roles of individual brain regions within such tasks activating the vision and valuation systems have been increasingly clarified using clever task designs and methodological approaches [7–11].

However, a fundamental gap in our knowledge lies in delineating how spatiotemporal patterns of neural responses in regions of the valuation and visual systems — as well as the whole brain more broadly — allow effective behavioral choices. While multivoxel pattern analysis and related techniques enable a local quantifi-

cation of regional representations of objects or concepts [12], developing tools that combine information across all brain regions and all processes (not simply representation, but also perception, action, and cognition) remains difficult. Put simply, we lack simple or intuitive heuristics to identify how structure in the combined activity of brain regions might reflect efficient cognition. We address this gap by using a geometric perspective, which represents distributed neural responses as points in a multidimensional space. Adapting tools from machine learning and data science [13], we study the task-based dimension, which measures how far apart neural responses to various stimuli are from each other during a task. We search for this intrinsic dimension of neural activity during training, hypothesizing that successful learners would retain a higher-dimensional activity profile, enabling greater separation between stimuli.

To test this hypothesis, we examine neural activity at the regional and voxel level, in a cohort of 20 healthy adult human subjects as they learned the values of 12 novel stimuli, and we ask how the dimension of their neural responses reflected learning speed. Across four days of task practice, participants learned the monetary values of twelve three-dimensional computer-generated shapes through feedback, while their blood oxygen level dependent (BOLD) functional MRI data were collected. We observed appreciable individual differences in the speed with which the participants learned these values [14]. We then use a generalized linear model to deconvolve the hemodynamic response function to obtain approximate

neural responses to each stimuli at the time points when they were presented; these responses were then spatially averaged in 83 regions of interest defined by a whole-brain anatomical parcellation. Finally, we study three notions of the geometry of the spatially embedded whole brain activity state, including the task-based and ambient dimensionality, and assortativity of the pattern of neural responses, with the goal of providing a mathematical corollary to the notion of cognitive coding efficiency.

We demonstrate that fast learners indeed have higher-dimensional task-based patterns of activity, allowing their neural responses to different stimuli to be more easily distinguished from one another. Furthermore, we identify brain regions that most contribute to the emergence of these high-dimensional patterns in quick learners. Next, we consider potential disadvantages of high dimensionality, which could require that the brain utilize more resources for the embedding of the information. For a quantitative assessment, we introduce the metric of ambient dimension: the dimension of neural activity that is agnostic to task information. We find that the ambient dimension of a fast learner is more compact than the ambient dimension of a slow learner, i.e. a more efficient embedding is utilized in successful learning. These findings illuminate the structure of neural responses to provide a notion of effective coding most associated with rapid learning: the use of a small ambient embedding to simultaneously encode high dimensional patterns of activity. Thus, we learn that fast learners have a pair of advantages: they begin with a more efficient embedding of possible features, and construct a richer set of distinguishing features from it. Lastly, as another lens on the structure of the neural responses, we ask how easy it is to distinguish between the observed neural responses. Thus, we investigate label assortativity, which captures another geometric property distinct from dimension. Our results confirm our prior analysis that fast learners have more distinguishable neural responses and our approach provides a suite of novel metrics to characterize their geometry.

RESULTS

Quick learners develop higher dimensional task-based neural responses

We seek to understand the relationship between a participant’s learning ability and the geometric structure of their neural responses. To examine this, we use whole-brain fMRI-BOLD data acquired from twenty humans (Fig. 1a; [14]) during one hour of task practice on each of four consecutive days. We then employ a generalized linear model to deconvolve the hemodynamic response function to obtain approximate neural responses to each stimuli at the time points when they were presented (Fig.

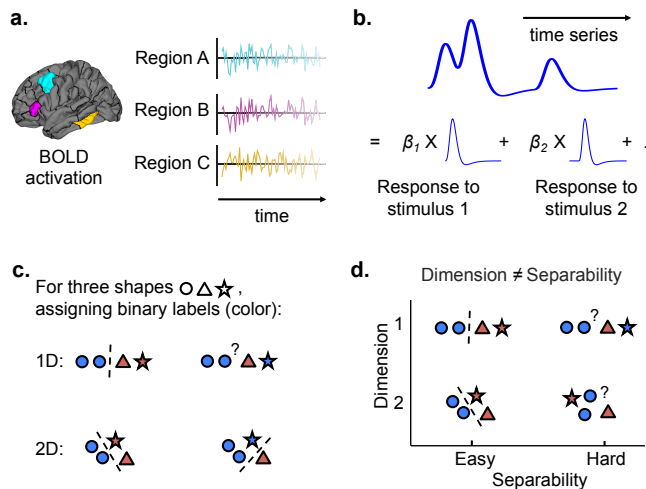


Figure 1: Neural responses from fMRI data; separability dimension and assortativity. **a.** We measure the fMRI-BOLD activation of different brain regions over time. **b.** We then use a generalized linear model to deconvolve the hemodynamic response function from the BOLD time series, to obtain approximate neural responses to each stimuli at the time points when they were presented. **c.** We assign binary labels (color) to the neural data (denoted by shapes). When the data are arranged in a low-dimensional manner (top row), some binary assignments will result in poor separability, whereas in a higher dimension, these binary assignments can be more easily separated. Binary separability is an estimate of separability dimension (see Methods). **d.** Separability dimension is distinct from the assortativity of the original labels, which can measure a different geometric aspect of the same data set.

1b; Methods). Responses were spatially averaged in 83 regions of interest defined by a whole-brain anatomical parcellation.

The dimensionality of the evoked responses can be estimated based on the performance of a linear classifier in distinguishing assigned binary labels on the data (see Fig. 1c; Methods). For n stimuli, there are $\binom{n}{n/2} - 2$ ways of creating a binary re-labeling of the neural responses [13]. When the data are arranged in a low-dimensional manner, some binary assignments will result in poor separability, whereas in a higher dimension, these binary assignments remain separable (Fig. 1c). Hence, we average over the result from all these binary labels to obtain our estimate, which is the *task-based separability dimension*. Note that this averaging over many separating hyperplanes ensures the robustness of this method under noise – any particular plane might suffer from a perturbation, however the average will be stable.

For $n = 12$, $\binom{12}{6} - 2$ binary assignments become computationally expensive, hence in practice we choose a subset of $m = 4$ stimuli over which to calculate this separability dimension. To ensure that our results do not depend on the particular subset of stimuli chosen, we use

20 different combinations (roughly 7%) out of the $\binom{n}{m}$ available choices, making sure that each shape was represented an equal number of times throughout these 20 combinations.

This approach was applied to the evoked neural responses of participants learning the value of twelve shapes, each associated with a different monetary value (see Fig. 2a). At each trial, participants were shown a pair of shapes simultaneously and asked to select which shape had the higher value, after which they received feedback based on their response (see Fig. 2b). There were three such learning sessions per day across four days (see Fig. 2c), as well as additional sessions where retention was assessed by having subjects judge the value of individual shapes (see Methods; [14]). We focus on these latter value judgment sessions conducted at the end of each day, where stimuli were presented singly and hence we can isolate neural responses to each shape. As a metric for the real-time learning ability of participants, we choose their response accuracy at the end of the first day, where we observed the greatest individual variability (see Fig. 2c).

As we are interested in how the geometry of subject’s neural responses changes with learning, we investigate the task-based separability dimension of their neural activity at the end of the experiment: that is, on the fourth and final day of training. We find that the response accuracy of participants at the end of the first day of training is significantly correlated with their separability dimension (see red points with error bars in Fig. 3a). For statistical comparison, we construct a null model by randomly permuting the assignment of shapes to neural responses, and then calculate the same metric on these data with scrambled labels, which is the ambient separability dimension. Compared to bootstrapped samples from the null data (gold bar in Fig. 3a), we observe that the correlation $r = 0.56$ from the task-based data was significant with non-parametric $p < 0.001$. Intuitively, this finding suggests that participants who learn more quickly also display a larger task-based separability dimension of their neural representation.

Quick learners have a lower ambient dimension and hence more efficient neural responses

Intuitively, a high-dimensional response could provide flexibility but is naturally more computationally intensive, while a low-dimensional response is simpler, but rigid. How do quick learners balance both these aspects in developing efficient neural responses? To understand this, we extend our calculations from the previous section across a range of values of m . We calculate the correlation between separability dimension and learning ability for the real task-based data and for the null data for 100 bootstrapped samples, up to $m = 10$ (see Fig. 3b; Meth-

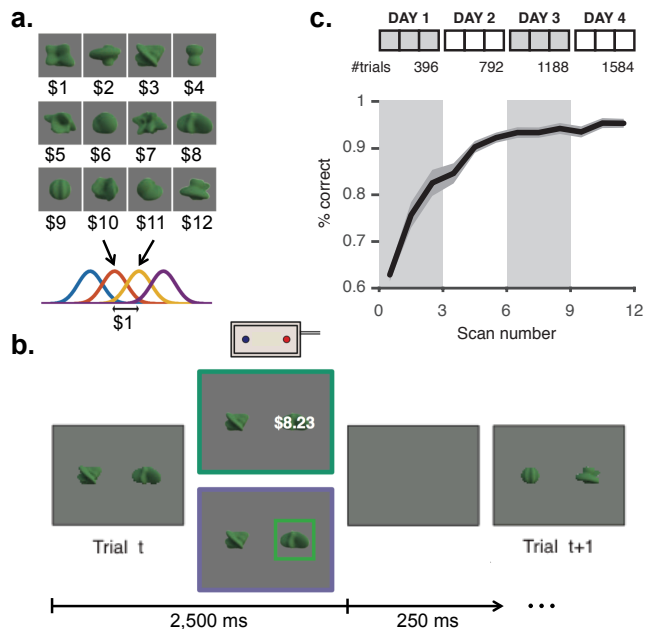


Figure 2: Experimental protocol and behavioral results. **a.** Stimulus set and corresponding values. Twelve abstract shapes were computer generated, and an integer value between \$1 and \$12 was assigned to each. On each trial, the empirical value of each shape was drawn from a Gaussian distribution with fixed mean (i.e., the true value), and standard deviation of \$0.50. **b.** Task paradigm. Participants were presented with two shapes side-by-side on the screen and asked to choose the shape with the higher monetary value. Once a selection was made, feedback on their selection was provided. Each trial lasted 2.75 s (250 ms inter-stimulus interval). **c.** The experiment was conducted over four consecutive days, with three experimental scans (396 trials) on each day, for a total of 1584 trials. Learning was conducted over four days, with three training sessions per day. Participants’ accuracy in selecting the shape with higher expected value improved steadily over the course of the experiment, increasing from chance level in the first few trials to approximately 95% in the final few trials ($N = 16$).

ods). Here, we notice that the real data are consistently more positively correlated (red points) and fall far outside the error bars of the null data (gold points), confirming that the real data reflects quick learners having a higher separability dimension of their neural responses, for all choices of m . This becomes particularly clear at large m where the combinatorics of $\binom{m}{m/2} - 2$ binary assignments that are averaged over for each calculation, leads to a strong convergence of the results as reflected in very small error bars.

We now turn to the separability dimension of the null data, which has a distinct and interesting interpretation. It is also the *ambient dimension*, i.e. the embedding space within which the task-based variables are encoded. This ambient separability dimension shows the opposite trend: it is negatively correlated with the response ac-

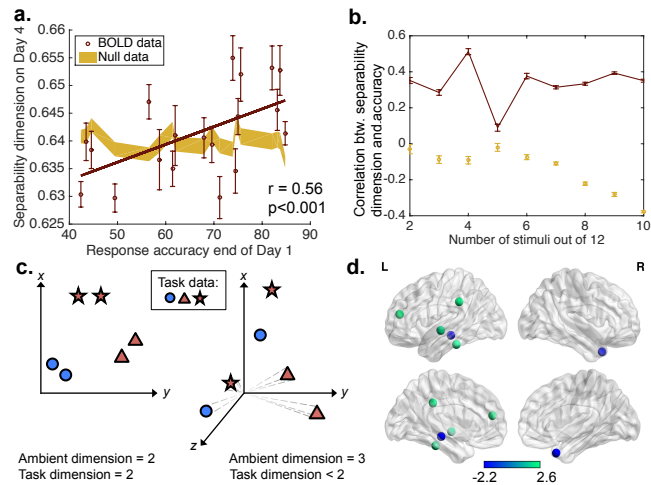


Figure 3: Quick learners show a more efficient neural representation – larger task-based dimension but smaller ambient dimension. **a.** Correlation of separability dimension of neural representation for $m = 4$ with learning accuracy across participants. Red markers denote the real data, showing a positive correlation of $r = 0.56$, with non-parametric $p < 0.001$ compared to the shuffled data (null model), which has error bars shown in gold. **b.** Correlation of separability dimension with learning accuracy across subjects, for m from 2 to 10 (see Methods); the true data is in red while the shuffled data (null model) is in gold (same color scheme as **a.**). We see that the true data always falls outside the error bars of the null model, and that the former shows a positive correlation while the latter, a negative correlation – suggesting that participants who learn more quickly have a larger task-based dimension but smaller ambient dimension of their neural representation. **c.** Schematic of how data can have a simultaneously larger task dimension with smaller ambient dimension, which is more efficient (left), and *vice versa* (right); x , y and z are distinct measurements. In this cartoon, quick learners would have neural responses similar to the left, while slow learners would have neural responses similar to the right. **d.** A virtual lesioning experiment shows which brain regions most weaken this result upon their removal (blue, z -score < -2), as well as which brain regions most enhance this result upon their removal (green, z -score > 2).

curacy of participants (gold points in Fig. 3b). These observations indicate that the ambient dimension of mislabelled data is instead smaller for quick learners, who also have a larger dimension of their (correctly labelled) task-based neural responses. We provide a schematic of this relation in Fig. 3c, where shapes correspond to objects of different value, demonstrating how their organization can be simultaneously large given their real identity and yet compact within an ambient dimension. Together, these two features of quick learners indicate an overall efficient neural response: the delicate balance of ease in distinguishing task stimuli with the least amount of resources needed to encode such information. Lastly, we note that while all m values show this discrepancy

between the task-based and ambient separability dimension, given that $m = 4$ provides the strongest signal its computational efficiency compared to larger m , further calculations of separability dimension are conducted using $m = 4$.

Contribution of specific brain regions to individual learning ability

As a follow-up to understanding this main effect, we seek to determine which regions contributed the most to this enhanced dimension of neural representation observed in quick learners. To address this question, we conduct an exploratory analysis using a virtual lesioning approach, in which we calculate the binary separability of the neural responses and its correlation with participants’ response accuracy after removing a single region. By performing this calculation for each region, we can identify which region contributed most to the observed correlation. Here we report the regions whose absence most resulted in a change in the obtained correlation (magnitude of z -score > 2 or $p < 0.023$; uncorrected for multiple comparisons).

We find that the removal of the left hippocampus and right temporal pole causes the largest decreases in the observed correlation; hence, these regions contribute the most strongly to the association between learning ability and separability dimension of neural response (blue regions in Fig. 3d). In other words, in subjects that learn quickly, the left hippocampus and right temporal pole seem to contribute to a higher separability dimension and *vice versa*. A possible explanation for these results is that learning to perform this task requires effective separability of stimulus dimensions mediated by these regions. In line with these results, the hippocampus is known to play a key role in the rapid learning of stimulus associations [15], and the temporal pole to represent information about abstract conceptual properties of objects (such as object value) [16]. In contrast, the removal of regions such as the left rostral middle frontal cortex and left supramarginal gyrus (green regions in Fig. 3d) enhances the observed correlation, suggesting that their activity is orthogonal to or does not directly contribute to the large separability dimension that characterizes quick learners. Generically, we expect orthogonal signals to reduce the correlation – as the addition of an unrelated signal to a signal of interest will damage the correlation to that target signal.

Quick learners show high dimensional task-based neural responses within local brain regions

We can further ask, what is the geometry of the neural response pattern within individual brain regions, across

voxels? Are relations between learning and dimensionality in the whole brain replicated also on a smaller scale, thus suggesting some degree of scale invariance? Or are there other regions that do not repeat these patterns at the voxel-level, and what does that tell us about the relative engagement of those regions in learning of object value?

Up to this point, we have studied neural activity across the whole-brain and the separability dimension of such neural activity. It is natural to ask if this relationship between learning ability and the dimension of neural responses can also be found in local sections of the activity data. To address this question, we adapt the analysis to examine ten brain regions of 300 (or fewer) voxels (see Methods) chosen based on their hypothesized relevance to the task, and we study the separability dimension of neural data from these parcels. In this case, we examine the correlation of separability dimension in the neural data in each local region with the participants’ response accuracy on day 1, as before. We find that three regions show significant positive correlation compared to the null model of shuffled data, with non-parametric $p \leq 0.05$: see Fig. 4a, b. These are the left anterior cingulate and primary visual cortices, as well as the right posterior fusiform cortices, respectively, where the first region passes $p \leq 0.05$ corrected for multiple comparisons (see Table I).

Notably, the anterior cingulate cortex is thought to play a role in reward-based learning [17], while the visual areas V1 and posterior fusiform are involved in the representation of lower-level and higher-level features of objects, respectively [18]. Our findings therefore suggest that these regions are comparatively more engaged in the creation of a value-related heuristic at a local level, and are consistent with previous work showing that the right and left posterior fusiform exhibit differential responses during object recognition [19–21].

TABLE I: Brain regions where a larger dimension of neural activity is correlated with learning ability.

The left anterior cingulate passes $p < 0.005$ corrected for multiple comparisons (marked with *).

No. of voxels	Brain region	Hemisphere	r	p
300	Anterior cingulate	Left	0.54	0.003*
300	Primary visual	Left	0.49	0.016
300	Posterior fusiform	Right	0.61	0.050

Quick learners develop more assortative patterns of neural responses

Besides separability dimension, a complementary geometric approach is that of *label assortativity*, which simply identifies how easily distinguishable the neural re-

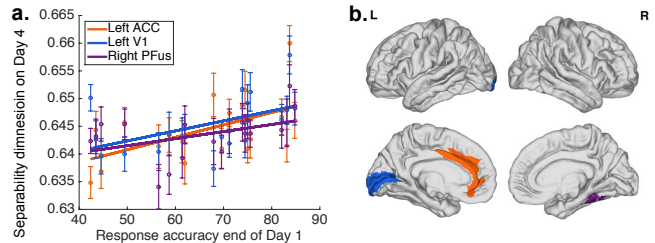


Figure 4: Quick learners show a larger dimension of responses in certain key regions at the voxel level. a.

We study regions of 300 (or fewer) voxels that we hypothesize to be involved in the processing of value and the learning of shapes. We see that three regions show this positive correlation between learning accuracy and separability dimension in that region, with non-parametric $p \leq 0.05$ compared to the scrambled data (null models). **b.**

These three brain regions on a map of the brain: the left anterior cingulate cortex, left primary visual area, and right posterior fusiform.

sponses are from each other (according to all labels, and not just binarized labels). These two approaches provide distinct and potentially independent metrics on how these data are organized (see Fig. 1d). In our learning data, we hypothesize that quick learners should show a larger assortativity of their data, in addition to a larger separability dimension (see Fig. 5a). Here, we calculate assortativity using a linear support vector machine, chosen because of its simple interpretability.

When examining the same neural data from the value judgement session at the end of the fourth day, and comparing that with the response accuracy of participants on the first day, we find a positive correlation with their assortativity. Comparing this correlation to that observed in the null model in which labels are randomly permuted, we find that this correlation of $r = 0.55$ is significant with non-parametric $p = 0.012$ (see Fig. 5b), i.e. participants who learn more quickly have a more assortative pattern of neural responses. To verify that the metrics of separability dimension and label assortativity do not have a strict overlap, we verify that one metric explains $r^2 = 34\%$ of the variance of the other.

DISCUSSION

In this study, we develop intuitive and interpretable metrics to quantify the geometric organization of neural activity, that characterizes quick learners as they learn the value of novel stimuli. To do this, we draw on methods from machine learning and data science [13] to estimate the intrinsic dimension of noisy measurements, and introduce the new metrics of task-based and ambient dimension, respectively. In a cohort of 20 humans in a value-learning experiment consisting of four days of training, we find that participants who learn most quickly dis-

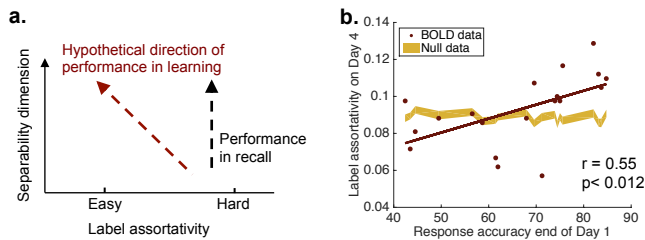


Figure 5: Dimension and assortativity provide a geometric picture of neural data. **a.** As different cognitive processes can exhibit typified geometric changes in the neural responses to various stimuli, we hypothesize that performance by humans in value learning would be associated with higher dimension and assortativity. In a recall task, successful performance in macaques is associated with higher dimension but not assortativity [13]. **b.** The distinct metric of label assortativity (according to all labels; see Fig. 1d) across the whole brain, shows that quick learners also display a higher assortativity ($r = 0.55$; red markers), compared to the shuffled data in gold with non-parametric $p = 0.012$.

play uniquely optimized neural responses to encode the cognitive processes (including, perception and decision-making) associated with the task – achieving a delicate and efficient balance of a large task-based dimension and small ambient dimension, respectively. We apply these tools both at the whole-brain and at the voxel levels, providing a lens through which to examine the relationship of this organization on different scales. With the inclusion of label assortativity, our work offers a suite of tools to characterize the geometric organization of neural activity, that can distinguish between the performance of individuals during a quintessential task of learning values given external feedback.

A notion of cognitive coding efficiency. Extending previous methods, we introduce various types of dimension (ambient and task-based, respectively) that allow insight into learning capacity and flexibility. Our results are consistent with the notion that the substantially different use of these two types of dimension could allow efficient encoding of contextually relevant data, potentially supporting optimal learning strategies. The compression of a large amount of information or content into as small a space as possible is done on all levels of biology from densely coiled DNA to sensory neural systems [2]. Our results suggest that similar principles of efficiency may also operate on the level of cognition or higher-order neural processes.

Related concepts have proven highly effective at the neuronal level, where prior work demonstrates the utility of characterizing dimension in neural representations. For example, data from the lateral intraparietal area in macaques suggests that neuronal spiking maps onto a one-dimensional dynamical trajectory [22]. This theory has allowed powerful and counter-intuitive interpreta-

tions about disparate cognitive processes from decision-making and attentional shifting, to biased representations that arise from associative learning [23]. Intriguingly, in the recall task studied in [13], the estimated dimension from activity in the prefrontal cortex is higher when the macaque responds correctly. Qualitatively, this finding is consistent with our own work in humans: that is, the dimension of neural activity can be used to predict the animal’s performance.

It is also of interest to ask whether these geometric notions could provide insights into the quantitative similarities and differences between distinct cognitive processes elicited by various tasks. In a previous experiment examining recall performance in trained macaques, the two estimates of dimension and decoding accuracy (analogous to separability) are differentially related to behavior [13]. Specifically, while the dimension of the macaque’s neural representation was predictive of the macaque’s performance, the decoding accuracy of the same neural data instead remained constant in both error and correct trials. These observations raise fundamental questions about whether different cognitive processes can exhibit typified geometric changes in the neural responses.

Role of single regions within a broader whole-brain geometry. On the level of local brain regions, we find that the left primary visual and anterior cingulate cortices, and right posterior fusiform of quick learners display this differential increase in dimension. This finding is in contrast to role of these same regions in the opposite hemisphere – where the latter is consistent with previous studies on lateralization in the fusiform area during object recognition [19–21]. Meanwhile, our other results suggest that such lateralization may be present in the anterior cingulate or primary visual cortices as well, providing suggestions for experimental verification.

Methodological considerations. While characterizing aspects of the geometry, this work does not identify the exact topology of the response, even while dimension and assortativity provide important starting points for a deeper analysis. In addition, these broad geometric methods would also be well-complemented by a dynamical study to assess how this geometry evolves across time. Lastly, while our cohort of twenty subjects already demonstrates significant evidence for geometric features that distinguish quick from slow learners, these results can be verified across larger samples and in other experimental paradigms.

Concluding remarks. The tools that we develop and exercise here hold promise for the analysis of complex cognitive tasks due to their applicability in non-invasive neuroimaging and robustness to noise. Indeed, in principle our tools provide a broad and uniform characterization of data structure that could be used to compare outcomes between cognitive tasks. Further work could probe experiments carried out over different scales (of space and time) to investigate commonalities or to create more com-

plete descriptions. Importantly, such comparisons are in principle made possible by the fact that while the absolute value of these metrics depends on the particular measurement technique, relative changes in value could be used to compare between data collected using measurement techniques, during the different experiments, or as different cognitive processes are engaged. It would be particularly interesting in future to use these geometric tools to quantitatively compare and contrast the mental states engendered by “explore” *versus* “exploit” behaviors common in general human experience, which are thought to give rise to diffuse *versus* structured neural representations.

-
- [1] Barlow, H. Possible principles underlying the transformations of sensory messages. In *Sensory Communication* (1961).
- [2] Olshausen, B. A. & Field, D. J. Sparse coding with an overcomplete basis set: A strategy employed by v1? *Vision Research* **37**, 3311 – 3325 (1997).
- [3] Buzsáki, G. & Watson, B. O. Brain rhythms and neural syntax: implications for efficient coding of cognitive content and neuropsychiatric disease. *Dialogues Clin Neurosci* **14**, 345–367 (2012).
- [4] Haier, R. J., Siegel, B., Tang, C., Abel, L. & Buchsbaum, M. S. Intelligence and changes in regional cerebral glucose metabolic rate following learning. *Intelligence* **16**, 415 – 426 (1992).
- [5] Poldrack, R. A. Is efficiency a useful concept in cognitive neuroscience? *Developmental Cognitive Neuroscience* **11**, 12 – 17 (2015).
- [6] Felleman, D. J. & Van Essen, D. C. Distributed hierarchical processing in the primate cerebral cortex. *Cerebral Cortex* **1**, 1–47 (1991).
- [7] Grill-Spector, K. & Malach, R. The human visual cortex. *Annual Review of Neuroscience* **27**, 649–677 (2004). PMID: 15217346.
- [8] Bartra, O., McGuire, J. T. & Kable, J. W. The valuation system: A coordinate-based meta-analysis of BOLD fMRI experiments examining neural correlates of subjective value. *NeuroImage* **76**, 412 – 427 (2013).
- [9] Op de Beeck, H. P. *et al.* Fine-scale spatial organization of face and object selectivity in the temporal lobe: Do functional magnetic resonance imaging, optical imaging, and electrophysiology agree? *Journal of Neuroscience* **28**, 11796–11801 (2008).
- [10] Grill-Spector, K. & Weiner, K. S. The functional architecture of the ventral temporal cortex and its role in categorization. *Nat Rev Neurosci* **15**, 536–548 (2014). Review.
- [11] Cohen, M., Heller, A. & Ranganath, C. Functional connectivity with anterior cingulate and orbitofrontal cortices during decision-making. *Cognitive Brain Research* **23**, 61 – 70 (2005). Multiple Perspectives on Decision Making.
- [12] Kahnt, T. A decade of decoding reward-related fMRI signals and where we go from here. *Neuroimage* **S1053-8119**, 30468–8 (2017).
- [13] Rigotti, M. *et al.* The importance of mixed selectivity in complex cognitive tasks. *Nature* **497**, 585–590 (2013).
- [14] Mattar, M. G., Thompson-Schill, S. L. & Bassett, D. S. The network architecture of value learning. *Network Neuroscience* **0**, 1–27 (2017).
- [15] Squire, L. R. Memory and the hippocampus: a synthesis from findings with rats, monkeys, and humans. *Psychological review* **99**, 195 (1992).
- [16] Peelen, M. V. & Caramazza, A. Conceptual object representations in human anterior temporal cortex. *Journal of Neuroscience* **32**, 15728–15736 (2012).
- [17] Bush, G. *et al.* Dorsal anterior cingulate cortex: a role in reward-based decision making. *Proceedings of the National Academy of Sciences* **99**, 523–528 (2002).
- [18] Grill-Spector, K. The neural basis of object perception. *Current Opinion in Neurobiology* **13**, 1–8 (2003).
- [19] Vuilleumier, P., Henson, R. N., Driver, J. & Dolan, R. J. Multiple levels of visual object constancy revealed by event-related fmri of repetition priming. *Nat Neurosci* **5**, 491–499 (2002).
- [20] Koutstaal, W. *et al.* Perceptual specificity in visual object priming: functional magnetic resonance imaging evidence for a laterality difference in fusiform cortex. *Neuropsychologia* **39**, 184 – 199 (2001).
- [21] Simons, J. S., Koutstaal, W., Prince, S., Wagner, A. D. & Schacter, D. L. Neural mechanisms of visual object priming: evidence for perceptual and semantic distinctions in fusiform cortex. *NeuroImage* **19**, 613 – 626 (2003).
- [22] Ganguli, S. *et al.* One-dimensional dynamics of attention and decision making in LIP. *Neuron* **58**, 15 – 25 (2008).
- [23] Fitzgerald, J. *et al.* Biased associative representations in parietal cortex. *Neuron* **77**, 180–191 (2013).
- [24] Ward, G. J. The radiance lighting simulation and rendering system. In *Proceedings of the 21st Annual Conference on Computer Graphics and Interactive Techniques, SIGGRAPH '94*, 459–472 (ACM, New York, NY, USA, 1994).
- [25] Dale, A. M., Fischl, B. & Sereno, M. I. Cortical surface-based analysis: I. segmentation and surface reconstruction. *Neuroimage* **9**, 179–194 (1999).
- [26] Greve, D. N. & Fischl, B. Accurate and robust brain image alignment using boundary-based registration. *Neuroimage* **48**, 63–72 (2009).
- [27] Jenkinson, M. Improving the registration of b0-distorted epi images using calculated cost function weights. In *Tenth International Conference on functional mapping of the human brain* (2004).
- [28] Jenkinson, M., Bannister, P., Brady, M. & Smith, S. Improved optimization for the robust and accurate linear registration and motion correction of brain images. *Neuroimage* **17**, 825–841 (2002).
- [29] Smith, S. M. Fast robust automated brain extraction. *Human brain mapping* **17**, 143–155 (2002).
- [30] Friston, K. J., Williams, S., Howard, R., Frackowiak, R. S. & Turner, R. Movement-related effects in fmri time-series. *Magnetic resonance in medicine* **35**, 346–355 (1996).
- [31] Behzadi, Y., Restom, K., Liau, J. & Liu, T. T. A component based noise correction method (compcor) for bold and perfusion based fmri. *Neuroimage* **37**, 90–101 (2007).
- [32] Jo, H. J., Saad, Z. S., Simmons, W. K., Milbury, L. A. & Cox, R. W. Mapping sources of correlation in resting state fmri, with artifact detection and removal. *Neuroimage* **52**, 571–582 (2010).
- [33] Murphy, K., Birn, R. M., Handwerker, D. A., Jones, T. B.

- & Bandettini, P. A. The impact of global signal regression on resting state correlations: are anti-correlated networks introduced? *Neuroimage* **44**, 893–905 (2009).
- [34] Saad, Z. S. *et al.* Trouble at rest: how correlation patterns and group differences become distorted after global signal regression. *Brain connectivity* **2**, 25–32 (2012).
- [35] Chai, X. J., Castañón, A. N., Öngür, D. & Whitfield-Gabrieli, S. Anticorrelations in resting state networks without global signal regression. *Neuroimage* **59**, 1420–1428 (2012).
- [36] Power, J. D., Schlaggar, B. L. & Petersen, S. E. Recent progress and outstanding issues in motion correction in resting state fmri. *Neuroimage* **105**, 536–551 (2015).
- [37] Murphy, K. & Fox, M. D. Towards a consensus regarding global signal regression for resting state functional connectivity mri. *NeuroImage* (2016).
- [38] Daducci, A. *et al.* The connectome mapper: An open-source processing pipeline to map connectomes with mri. *PLOS ONE* **7**, 1–9 (2012).
- [39] Julian, J. B., Fedorenko, E., Webster, J. & Kanwisher, N. An algorithmic method for functionally defining regions of interest in the ventral visual pathway. *Neuroimage* **60**, 2357–2364 (2012).
- [40] Glasser, M. F. *et al.* A multi-modal parcellation of human cerebral cortex. *Nature* **536**, 171–178 (2016).
- [41] Power, J. D. *et al.* Functional network organization of the human brain. *Neuron* **72**, 665–678 (2011).

METHODS

Estimating separability dimension from data with binary labels

Given several types of data, e.g. the shapes in Fig. 1c (where there can be several measures of the same shape), we can assign a binary label to each shape (represented by the color). In our case, the types of data are the different responses to n stimuli. And for n stimuli/ types of responses, there will be $\binom{n}{n/2}$ ways to assign binary labels to these data [13]. We can then ask how separable are these binary categories, across all $\binom{n}{n/2}$ relabellings? We can see that when the data is arranged in one dimension, it becomes hard to separate the binary categories in all but one of the binary assignments. When the data is in a higher dimension, it will tend to be easier to separate these binary categories. Hence the average binary separability will estimate the separability dimension of the data.

We perform this analysis on m subsets of the stimuli: that is, for m stimuli out of the 12 there are $\binom{12}{m}$ ways, where we choose 20 draws out of the different possible combinations in a uniform way (so that each stimuli is represented a similar number of times). This can be done for $m = 2, \dots, 10$, where $\binom{12}{m} > 20$, and in order to preserve statistical rigor we do not go past $m = 10$ as there would be fewer draws for $m = 11$ and 12. We also choose to use $m = 4$ as a mid-size subset for efficient computation for all our calculations, except in Fig. 3b where we

show results for all $m \leq 12$ to verify that the conclusions remain similar.

Linear SVM and cross validation

In calculating binary separability, the MATLAB linear support vector machine (SVM) is used with cross-validation by partitioning the data in five folds. For each fold, a model was trained using the out-of-fold observations, after which model performance was assessed using in-fold data. The average test error is calculated over all folds to provide an estimate of the predictive accuracy of the final model, and is used as the measure of binary separability. A similar cross-validation procedure is used to calculate label assortativity, where in this case the MATLAB linear SVM is also used with the data retaining all $n = 12$ distinct labels.

Value-learning experiment

Participants

Twenty human participants (nine female; ages 19–53 years; mean age = 26.7 years) with normal or corrected vision and no history of neurological disease or psychiatric disorders were recruited for this experiment. All participants volunteered and provided informed consent in writing in accordance with the guidelines of the Institutional Review Board of the University of Pennsylvania (IRB #801929). Participants had no prior experience with the stimuli or the behavioral paradigm.

Experiment

All subjects learned the monetary value of 12 novel visual stimuli over the course of four consecutive days (Fig. 2a; [14]). On each trial of the experiment, participants selected which of two shapes simultaneously present on the screen had the highest value, after which they received feedback based on their response (Fig. 2b). Although each shape had a true value, the empirical value used for each trial was drawn from a Gaussian distribution with a fixed mean (i.e., true value; Fig. 2a) and with a standard deviation of \$0.50. The average accuracy in selecting the shape with the highest mean value at each trial gradually improved over the course of the experiment, increasing from approximately 50% (chance) in the first few trials to approximately 95% in the final few trials.

Stimuli

The novel stimuli were 3-dimensional shapes generated with a custom built MATLAB toolbox (code available at <http://github.com/saarela/ShapeToolbox>) and rendered with RADIANCE [24]. ShapeToolbox allows the generation of three-dimensional radial frequency patterns by modulating basis shapes, such as spheres, with an arbitrary combination of sinusoidal modulations in different frequencies, phases, amplitudes, and orientations. A large number of shapes were generated by selecting combinations of parameters at random. From this set, we selected twelve that were considered to be sufficiently distinct from one another. A different monetary value, varying from \$1.00 to \$12.00 in integer steps, was assigned to each shape. These values were uncorrelated with any parameter of the sinusoidal modulations, so that visual features were not informative of value.

On each trial of the experiment, participants were presented with two shapes side by side on the screen and asked to choose the shape with the higher monetary value in an effort to maximize the total amount of money in their bank. The shape values on a given trial were independently drawn from a Gaussian distribution with mean equal to the true monetary value and the standard deviation equal to \$0.50. This variation in the trial-specific value of a shape was incorporated in order to ensure that participants thought about the shapes as having worth, as opposed to simply associating a number or label with each shape.

Image Acquisition

We collected blood oxygen level dependent (BOLD) functional MRI data from each participant as they performed the task. A total of 12 scan runs over 4 days were completed by each person (three scans per session), totaling 1584 trials (Fig. 2c).

Participants completed 20 minutes of the main task protocol on each scan session, learning the values of the 12 shapes through feedback. The sessions were comprised of three scans of 6.6 minutes each, starting with 16.5 seconds of a blank gray screen, followed by 132 experimental trials (2.75 seconds each), and ending with another period of 16.5 seconds of a blank gray screen. Stimuli were back-projected onto a screen viewed by the participant through a mirror mounted on the head coil and subtended 4 degrees of visual angle, with 10 degrees separating the center of the two shapes. Each presentation lasted 2.5 seconds (250 ms inter-stimulus interval) and, at any point within a trial, participants entered their responses on a 4-button response pad indicating their shape selection with a leftmost or rightmost button press. Stimuli were presented in a pseudorandom sequence with every pair of shapes presented once per scan.

In addition to the main learning protocol, we collected fMRI data during a functional localizer, two scans of a size judgment task, and one scan of a value judgment task. No feedback was given in any of these tasks. The value judgment task scans consisted of consecutive presentations of shapes drawn from the set (1500 ms presentation and 250 ms inter-stimulus interval) as participants indicated whether the shape was one of the six least or one of the six most valuable shapes. The size judgment task scans consisted of consecutive presentations of shapes drawn from the set and presented with a $\pm 10\%$ size modulation (1500 ms presentation and 250 ms inter-stimulus interval) as participants indicated whether the shape was presented in a slightly larger or smaller variation.

Data from the value judgement scans (both the BOLD data and participants response accuracy) is what is analyzed in main text of the paper. In the value judgement session of the first day for one participant, the fMRI time series was poorly recorded due to a lack of synchronization between the computer and scanner. Hence this participant was excluded from the analyses, with the other 19 subjects contributing data for the main analyses described in this paper.

MRI data collection and preprocessing

Magnetic resonance images were obtained at the Hospital of the University of Pennsylvania using a 3.0 T Siemens Trio MRI scanner equipped with a 32-channel head coil. T1-weighted structural images of the whole brain were acquired on the first scan session using a three-dimensional magnetization-prepared rapid acquisition gradient echo pulse sequence (repetition time (TR) 1620 ms; echo time (TE) 3.09 ms; inversion time 950 ms; voxel size 1 mm \times 1 mm \times 1 mm; matrix size 190 \times 263 \times 165). A field map was also acquired at each scan session (TR 1200 ms; TE1 4.06 ms; TE2 6.52 ms; flip angle 60°; voxel size 3.4 mm \times 3.4 mm \times 4.0 mm; field of view 220 mm; matrix size 64 \times 64 \times 52) to correct geometric distortion caused by magnetic field inhomogeneity. In all experimental runs with a behavioral task, T2*-weighted images sensitive to blood oxygenation level-dependent contrasts were acquired using a slice accelerated multiband echo planar pulse sequence (TR 2,000 ms; TE 25 ms; flip angle 60°; voxel size 1.5 mm \times 1.5 mm \times 1.5 mm; field of view 192 mm; matrix size 128 \times 128 \times 80). In all resting state runs, T2*-weighted images sensitive to blood oxygenation level-dependent contrasts were acquired using a slice accelerated multiband echo planar pulse sequence (TR 500 ms; TE 30 ms; flip angle 30°; voxel size 3.0 mm \times 3.0 mm \times 3.0 mm; field of view 192 mm; matrix size 64 \times 64 \times 48).

Cortical reconstruction and volumetric segmentation of the structural data was performed with the Freesurfer

image analysis suite [25]. Boundary-Based Registration between structural and mean functional image was performed with Freesurfer *bbregister* [26]. Preprocessing of the resting state fMRI data was carried out using FEAT (FMRI Expert Analysis Tool) Version 6.00, part of FSL (FMRIB’s Software Library, www.fmrib.ox.ac.uk/fsl). The following pre-statistics processing was applied: EPI distortion correction using FUGUE [27]; motion correction using MCFLIRT [28]; slice-timing correction using Fourier-space time series phase-shifting; non-brain removal using BET [29]; grand-mean intensity normalization of the entire 4D dataset by a single multiplicative factor; highpass temporal filtering (Gaussian-weighted least-squares straight line fitting, with $\sigma=50.0s$).

Nuisance time series were voxelwise regressed from the preprocessed data. Nuisance regressors included (i) three translation (X, Y, Z) and three rotation ($pitch, yaw, roll$) time series derived by retrospective head motion correction ($R = [X, Y, Z, pitch, yaw, roll]$), together with expansion terms ($[R, R^2, R_{t-1}, R_{t-1}^2]$), for a total of 24 motion regressors [30]; (ii) the first five principal components of non-neural sources of noise, estimated by averaging signals within white matter and cerebrospinal fluid masks, obtained with Freesurfer segmentation tools and removed using the anatomical CompCor method (aCompCor) [31]; and (iii) an estimate of a local source of noise, estimated by averaging signals derived from the white matter region located within a 15 mm radius from each voxel, using the ANATICOR method [32]. Global signal was not regressed out of voxel time series due to its controversial application to resting state fMRI data [33–35]. In particular, the removal of global signal in our data could mask session-to-session variability in connectivity and potentially affect accurate estimation of long-distance connections, which are a major focus of our study. We instead follow recent guidelines that suggest that removing local white-matter signal and other non-neural sources are potential reasonable alternatives to global signal regression [36, 37].

GLM to extract stimuli responses from BOLD time series

From the BOLD time series of 0.5 Hz, we interpolate the data to obtain a time series corresponding to the frequency of presentation of stimuli during the value judgment session (at 1.75 s intervals). We then use a generalized linear model (GLM) to obtain the static responses to each of these stimuli for 184 stimuli in each sequence, see Fig. 1b. From here we keep the results for the first 140 stimuli shown in each session out of all 184 stimuli. This choice was dictated by the fact that the MRI acquisition does not continue past the length of hemodynamic response function for several of the last stimuli, thus providing inadequate data for decoding using the GLM.

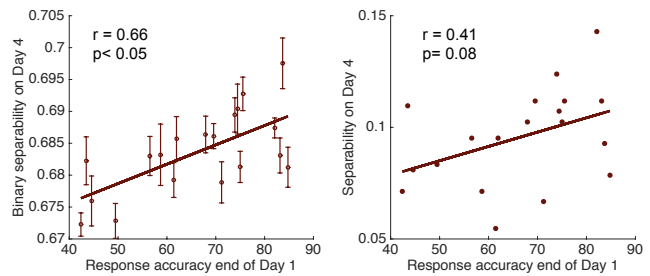


Figure 6: Replication of results using the whole-brain Power parcellation. *Left:* Separability dimension of neural responses on the fourth day is strongly correlated with the behavioral accuracy of subjects from the first day, with $r = 0.66$ and $p < 0.05$. *Right:* Label assortativity (retaining all twelve original labels) of the same data displays a positive trend with the response accuracy of subjects from the first day, with $r = 0.41$ and $p = 0.08$. These results are consistent with our results obtained on the Lausanne parcellation.

Whole-brain parcellation

For the whole-brain analyses, we subdivide participants’ gray matter volume into 83 cortical and subcortical areas (in both hemispheres), based on regions assigned from the Lausanne atlas [38]. For a replication of our results on a different whole-brain parcellation, please see our Supplementary Results.

Voxel level study of brain regions

We examine ten brain regions: posterior fusiform, anterior cingulate, orbito frontal, lateral occipital and primary visual cortices, each from the left and right hemisphere separately. We use the Group-Constrained Subject-Specific (GSS) method for defining the regions [39]. For each region, a large parcel is defined based on an existing parcellation [40], within which a maximum of 300 voxels with highest object-*versus*-scrambled t -statistic contrast from an independent localizer were selected. For lateral occipital and posterior fusiform, the parcels were downloaded from <http://web.mit.edu/bcs/nklab/GSS.shtml>. This procedure allowed the selection of ROIs that exhibited univariate responses to objects in a subject-specific manner.

REPLICATION OF RESULTS

We repeat our analyses on data obtained from a different whole-brain parcellation – a functional-based parcellation that subdivides the brain into 264 regions [41]. Note that because not all subjects had data in 3 out of the 264 regions, we retain the 261 brain regions common

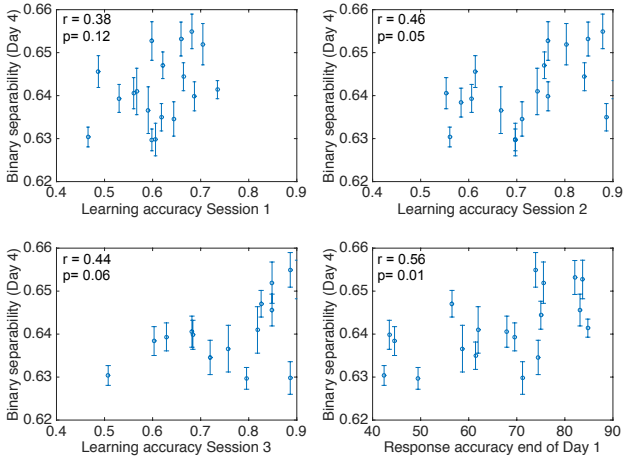


Figure 7: Emerging relationship between dimension of neural responses and behavioral accuracy. We examine how performance accuracy changes across the three learning sessions and value judgement session on the first day of training where the greatest individual differences were observed, and its correlations with separability dimension on the final day of training. We see that this correlation increases from $r = 0.28$ in the first learning session (top left) to $r = 0.56$ by the end of the first day in the value judgement session (bottom right).

to all participants. Upon repeating our calculations, we obtain similar results and conclusions, see Fig. 6.

SUPPLEMENTARY RESULTS

The emerging relationship between dimension of neural data and response accuracy

We also investigate how the learning of value emerges throughout the first day. We examine how the learning responses change across the three learning sessions and value judgement session on the first day, and ask whether individual differences in learning performance correlated with separability dimension on the last day of training (see Fig. 7). We find that the correlation between performance and separability increases from $r = 0.28$ in the first training session (Fig. 7, top left) to $r = 0.56$ by the end of the first day in the value judgement session (Fig. 7, bottom right), suggesting that this relationship

between the dimension of neural data and the response accuracy of participants emerges across sessions on the first day of training.

Comparison with size judgment

We can use our method on data from the size judgement session, which is very similar to the value judgement session in its setup and response format, but in which

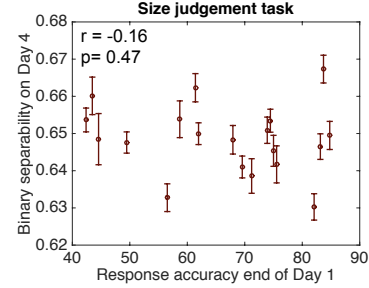


Figure 8: Dimension of neural data from size judgment sessions. The separability dimension of data from the size judgment task on the last day does not show significant differences between quick and slow learners, suggesting that the cognitive task or effort of judging value itself is necessary for this emergence of a larger dimensional neural response.

subjects are asked to evaluate the relative size of each shape (see Methods). Unlike for the neural responses in the value judgment session from the same day, we find that quick learners do not show any differences in their task-based separability dimension. Indeed, this separability dimension of neural data from the size judgment task shows no significant correlation with the response accuracy of subjects ($r = -0.16$, $p = 0.47$; see Fig. 8). These results show that neural responses to various shapes has a larger dimension for quick learners only when they are asked to evaluate or respond regarding the relative value of these shapes. This larger dimension is not evoked purely by visual apprehension of these shapes, suggesting that the cognitive task or effort of judging value itself is necessary for this emergence of a larger dimensional neural response.

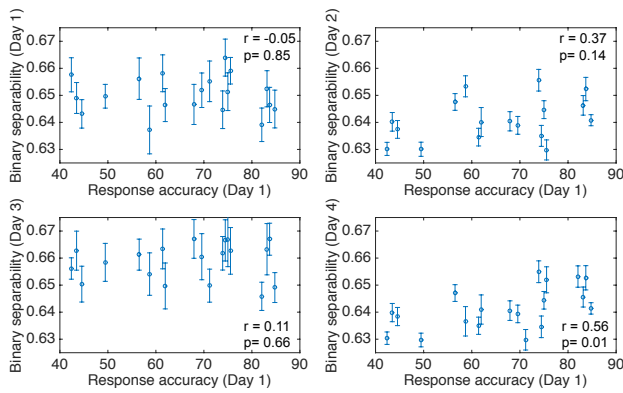


Figure 9: Changes of separability dimension across the four days. We study the correlation of the separability dimension of neural data from the value judgment sessions at the end of each day, with the response accuracy of participants on the first day. We find that quick learners do not have a particularly large dimension of neural response patterns on the first day, $r = -0.05$, $p = 0.85$, as compared to the fourth day, $r = 0.56$, $p = 0.01$, suggesting that this larger dimension for quick learners takes time to emerge.

Changes in separability dimension across the four days

We track the separability dimension of neural data from the value judgment sessions held at the end of each day, to calculate their correlation with the response accuracy of participants on the first day. We find that there is little correlation between the separability dimension of neural data and the performance on the first day, $r = -0.05$, $p = 0.85$, as compared to the fourth day, $r = 0.56$, $p = 0.01$, suggesting that this larger dimension of neural responses for quick learners also takes time to emerge.